catalysts

MDPI

Article

Efficient Cross-Coupling of Acetone with Linear Aliphatic Alcohols over Supported Copper on a Fluorite-Type $Pr_2Zr_2O_7$

Suhyun Lim [1,†], Minseok Kim [1,†], Sang Hyeok Ko [1], Jae-Hong Lee [1], Joon Hyun Baik [2] and Young-Woong Suh [1,3,*]

[1] Department of Chemical Engineering, Hanyang University, Seoul 04763, Korea
[2] Department of Chemical and Biological Engineering, Sookmyung Women's University, Seoul 04310, Korea
[3] Research Institute of Industrial Science, Hanyang University, Seoul 04763, Korea
* Correspondence: ywsuh@hanyang.ac.kr
† These authors contributed equally to this work.

Abstract: In cross-coupling of biomass-derived acetone and alcohols contributing to the production of carbon-elongated chemicals and fuels, the essential catalyst components are metal dispersion for alcohol dehydrogenation and, more importantly, basicity for carbon–carbon coupling. Herein, we report the potential of co-precipitated praseodymia–zirconia solid solution ($Pr_2Zr_2O_7$) as a support of Cu catalyst for the conversion of acetone and butanol into C_7 and C_{11} products. $Cu/Pr_2Zr_2O_7$ exhibits a high yield of C_7 and C_{11} (ca. 84%) compared to Cu/ZrO_2 and $Cu/PrO_{1.83}$. Moreover, it is robust under the employed solvent-free conditions owing to a solid solution of $Pr_2Zr_2O_7$ compared to $PrO_{1.83}$ showing phase transition to $PrOHCO_3$. It is also tolerant to up to 5 wt % water of the reactant mixture, recyclable once adequate post-treatment is employed after the reaction, and can convert the acetone–butanol–ethanol mixture into C_5–C_{11} products at the nearly equivalent yield (82%) to the acetone–butanol mixture. Therefore, the $Cu/Pr_2Zr_2O_7$ reported herein is an efficient catalyst for the coupling of acetone with linear aliphatic alcohols into biofuel precursors.

Keywords: cross-coupling; acetone; linear aliphatic alcohols; copper; $Pr_2Zr_2O_7$

Citation: Lim, S.; Kim, M.; Ko, S.H.; Lee, J.-H.; Baik, J.H.; Suh, Y.-W. Efficient Cross-Coupling of Acetone with Linear Aliphatic Alcohols over Supported Copper on a Fluorite-Type $Pr_2Zr_2O_7$. *Catalysts* **2022**, *12*, 1279. https://doi.org/10.3390/catal12101279

Academic Editor: Hiroto Yoshida

Received: 29 August 2022
Accepted: 19 October 2022
Published: 20 October 2022

1. Introduction

The acetone–butanol–ethanol (ABE) fermentation using the genus *Clostridium* has a long history because it produces fuels (ethanol and butanol) and chemicals (acetone, butyric acid, 1,3-propanediol, etc.) from various substrates such as glycerides, glycerol, carbon monoxide, and cellulose [1]. The first industrial ABE fermentation using the Weizmann process focused on acetone and butanol during World War I [2], and was then modified to meet the increasing demand of butanol [3]. However, its prominence declined in the middle of the twentieth century because of rapid advances in the petrochemical industry. In recent years, the ABE fermentation has gained renewed interest owing to the outstanding potential of bio-butanol as drop-in fuel [4,5]. Furthermore, Toste and coworkers suggested that the ABE mixture could be catalytically converted into hydrocarbon precursors of ketones and alcohols through carbon–carbon coupling [6]. Because the carbon number of these products possibly ranges from C_5 to C_{11}, they are compatible with existing fuel oils after oxygen removal.

In the first attempt, supported noble metal catalysts and basic K_3PO_4 were used together for the C–C coupling reaction [6]. The former component acts as a dehydrogenation site for the conversion of alcohols into aldehydes on the surface, and the latter's basicity initiates coupling of the formed aldehyde with acetone. When a mixture of acetone and butanol is used as the substrate, 2-heptanone and 6-undecanone are the products formed when acetone reacts with butanol in a mole ratio of 1:1 and 1:2, respectively. These ketones can be hydrogenated into alcohols by the hydrogen released by butanol dehydrogenation. Among the formed products, 6-undecanone and 6-undecanol are more desired than the C_7

products in terms of fuel efficiency. To produce C_{11} products selectively, the dehydrogenation reaction occurs at a higher rate, followed by coupling with acetone at a high efficiency. Therefore, a catalyst would be endowed with suitable metal dispersion and strong basicity, along with guaranteed catalyst stability under reaction conditions.

Sreekumar et al. [7] compared the activities of Pd, Ni, and Cu catalysts in alcohol dehydrogenation. Pd, along with soluble bases, is effective for the coupling of ketones with alcohols [7,8], yet the precious metal Pd needs to be replaced by first-row transition metals such as Cu and Ni. Zhu et al. [9] reported the improved water resistance of Ni–MgO–SiO_2 in the cross-coupling of the ABE mixture. Fridrich et al. [10] used Raney Ni catalyst with hydrotalcite-derived Mg–Al porous metal oxide (PMO) in the coupling of acetone with butanol. Moreover, supported Cu catalysts were effective in the reaction, where the formation of butyl butyrate caused by Lewis acidic Cu can be prevented by employing the supports with strong metal–support interaction, e.g., CeO_2–ZrO_2 [11] and CeO_2 [12].

Another important catalyst property is the basicity of supports used for metal loading. Basic sites of the aforementioned supports greatly influence the catalytic performance, although their acidity has moderate contribution. In pursuit of a new support, praseodymium oxide (praseodymia) is interesting because of its stronger basicity and metal–support interaction than CeO_2 [13–15]. Thus, it was used as a bulk catalyst for soot combustion [15], decomposition of 1,3-butanediol [16], and CO oxidation [17], and it could be employed as the support to load Pt [13], Ru [18], and Pd [19]. Furthermore, the cubic fluorite-type structure of praseodymia is facile in forming solid solutions by mixing with ceria [19–21], alumina [22], and zirconia [19,23], which can contribute to enhancement in catalyst stability. Despite these benefits, praseodymia and its mixed oxides have never been used for carbon–carbon coupling reactions.

Herein, the praseodymia–zirconia mixed oxide with the Pr/Zr mole ratio of 1:1 is prepared by co-precipitation together with single zirconia and praseodymia, where it is identified as disorder-defective fluorite-type $Pr_2Zr_2O_7$. The Cu catalysts supported on these supports are evaluated in the coupling of acetone with butanol. Their activities are discussed on the basis of physicochemical properties. Then, the effects of Cu loading, reaction time, and H_2O content present in the feed on the catalytic performance of Cu/$Pr_2Zr_2O_7$ are investigated. Furthermore, the recyclability of Cu/$Pr_2Zr_2O_7$ is examined, along with the possibility to use the ABE mixture as a feed. Consequently, the Cu/$Pr_2Zr_2O_7$ reported herein is assessed to be a possible catalyst system for efficient coupling of acetone with linear aliphatic alcohols.

2. Results and Discussion

2.1. Characteristics of Supported Cu Catalysts

The prepared Cu catalysts were characterized by X-ray diffraction (XRD) analysis for phase identification. As shown in Figure 1a, the fresh Cu/zirconia shows the major reflections assigned to monoclinic ZrO_2 (*m*-ZrO_2), along with a small reflection of tetragonal ZrO_2 (*t*-ZrO_2) at the 2θ of 30.3°. This is a result of using a strong basic solution for precipitation of zirconium species. At the same time, the reflection of Cu (111) is observed at the 2θ of 43.3°. In the case of the fresh Cu/praseodymia, the Cu (111) reflection is positioned at the same diffraction angle as for Cu/zirconia, whereas additional peaks are detected at the 2θ of 28.3°, 32.7°, 47.0°, 55.7°, and 58.4°. The measured XRD pattern was compared with the reference patterns of pure praseodymia phases, where praseodymium forms several stoichiometric and non-stoichiometric sub-oxides with formula PrO_x ($x \leq 2$) [13–15]. As a result of thorough examination, the XRD pattern turned out to be closer to the standard reflections of $PrO_{1.83}$ (JCPDS #06-0329) and Pr_6O_{11} (JCPDS #42-1121) than to those of PrO_2 (JCPDS #24-1006). The same finding was also reported for the praseodymia prepared by precipitation [24].

On the other hand, the fresh Cu/praseodymia–zirconia shows the reflections at the 2θ of 28.9°, 33.5°, 48.1°, 50.6°, 56.9°, and 60.0°, aside from the Cu peak at the 2θ of 43.3°. These peaks match the standard diffraction pattern of $Pr_2Zr_2O_7$ (JCPDS #19-1021). The

formula $A_2B_2O_7$, where A is a larger trivalent metal cation in eightfold coordination and B is a smaller tetravalent metal cation in sixfold coordination, represents a family of phases isostructural to the mineral pyrochlore [25]. The compound is normally observed when the radius ratio of A^{3+} to B^{4+} ranges from 1.46 to 1.78 [26]. The radius ratio of Pr^{3+} to Zr^{4+} in $Pr_2Zr_2O_7$ is 1.56 (=1.126 Å/0.72 Å), explaining that the reflections of $Pr_2Zr_2O_7$ are shifted toward high angles compared to pure praseodymia because the ionic radius of Zr^{4+} is smaller than that of Pr^{3+}. In addition, it was reported that $Pr_2Zr_2O_7$ exists in a disorder-defective fluorite or ordered pyrochlore structure [25], depending on the preparation method and annealing temperature [27,28]. In the XRD pattern of Cu/praseodymia–zirconia, superstructure diffraction peaks are absent, suggesting the formation of fluorite-type structure. From the above discussion, the Cu catalysts prepared in this work are hereafter denoted as Cu/*m*-ZrO_2, Cu/$PrO_{1.83}$, and Cu/$Pr_2Zr_2O_7$.

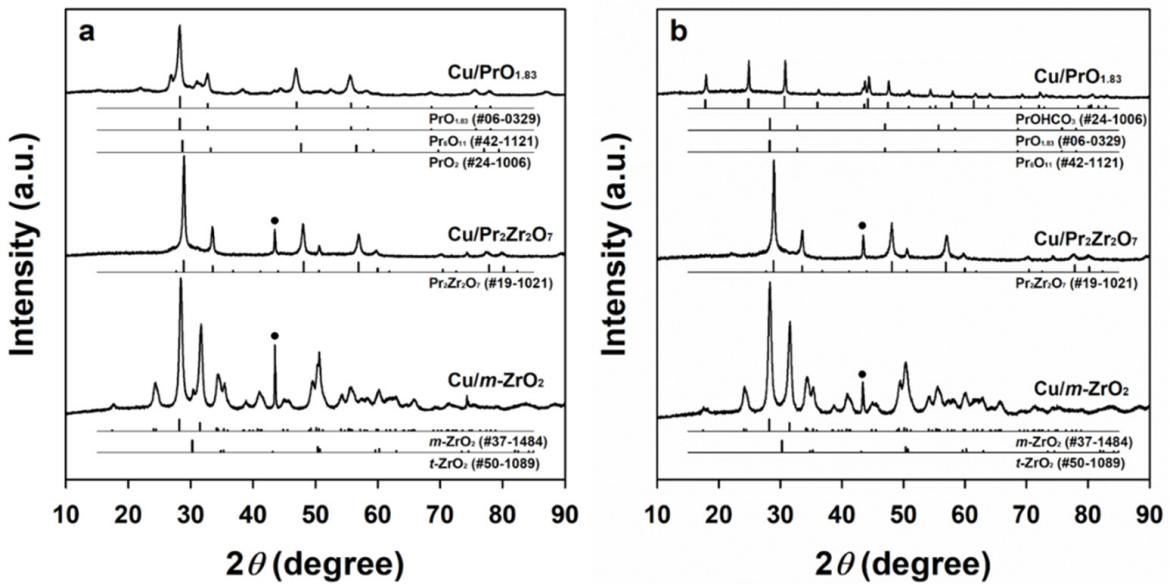

Figure 1. XRD patterns of (**a**) fresh and (**b**) spent Cu/m-ZrO_2, Cu/$Pr_2Zr_2O_7$, and Cu/$PrO_{1.83}$ catalysts. The symbol represents the diffraction peak of Cu (111) and the bar plots are the reference XRD patterns of $PrO_{1.83}$, Pr_6O_{11}, PrO_2, $PrOHCO_3$, $Pr_2Zr_2O_7$, m-ZrO_2, and t-ZrO_2.

The support materials and supported Cu catalysts were characterized by X-ray photoelectron spectroscopy (XPS) analysis (Figure 2). In the spectra of the Zr 3d core level, *m*-ZrO_2 shows the binding energies of Zr $3d_{3/2}$ and $3d_{5/2}$ peaks centered at 184.1 eV and 181.8 eV, respectively. The doublet is shifted to 183.7 eV and 181.4 eV for $Pr_2Zr_2O_7$. Such a shift is similarly observed in between Cu/*m*-ZrO_2 and Cu/$Pr_2Zr_2O_7$. The shift towards a lower binding energy indicates electron enrichment of Zr^{4+} by Pr species. In the spectra of the O 1s core level, the peak around 531 eV represents the loosely bound surface oxygen species (O_{ads}) and the peak at the lower binding energy can be assigned to the surface lattice oxygen (O_{lat}) [29]. While the peak of O_{ads} at 530.9 eV is negligibly changed, the peaks of O_{lat} in the spectra of *m*-ZrO_2, $Pr_2Zr_2O_7$, and $PrO_{1.83}$ are positioned around 529.2 eV, 528.6 eV, and 528.1 eV, respectively. The similarity is found in the O 1s spectra of the supported Cu catalysts. The trend in the binding energy of O_{lat} is attributed to the higher electronegativity of Zr^{4+} (1.3) than Pr^{3+} (1.13).

The more interesting result is that the fraction of O_{ads} increases with the Pr composition. This is in accordance with the results reported for Pr-doped CeO_2 [30] and In_2O_3 [31]. When the two deconvoluted curves are integrated, the area ratio $O_{ads}/(O_{ads} + O_{lat})$ increases from 28.9% of *m*-ZrO_2 to 51.2% of Pr_2ZrO_7 and further to 91.2% of $PrO_{1.83}$, which is similarly observed in the spectra of the supported Cu catalysts. In the report of Zhang et al. [32], this ratio was used to estimate the amount of oxygen vacancy. In the case of Pr-containing samples, the O_{ads} peak originates from the oxygen species in O–Pr^{3+}

bonds. When deconvoluted using the curve fitting reported for Pr_6O_{11} [33], the presence of Pr^{3+} is identified at 932 eV and 927.2 eV in $Pr_2Zr_2O_7$, $PrO_{1.83}$, and their supported Cu catalysts. Therefore, a number of oxygen vacancies are present in $PrO_{1.83}$ due to the high basicity of Pr. However, this might be problematic in CO_2-releasing reactions because the oxygen vacancy can contribute to the adsorption of CO_2 [34]. Since the transformation of CeO_2 to $CeOHCO_3$ was found in Cu–CeO_2 [12], the number of oxygen vacancies in $PrO_{1.83}$ may need to be reduced by mixing with Zr^{4+}, that is, $Pr_2Zr_2O_7$. In contrast, zirconia with the low $O_{ads}/(O_{ads} + O_{lat})$ is not highly basic for the reaction studied in this work.

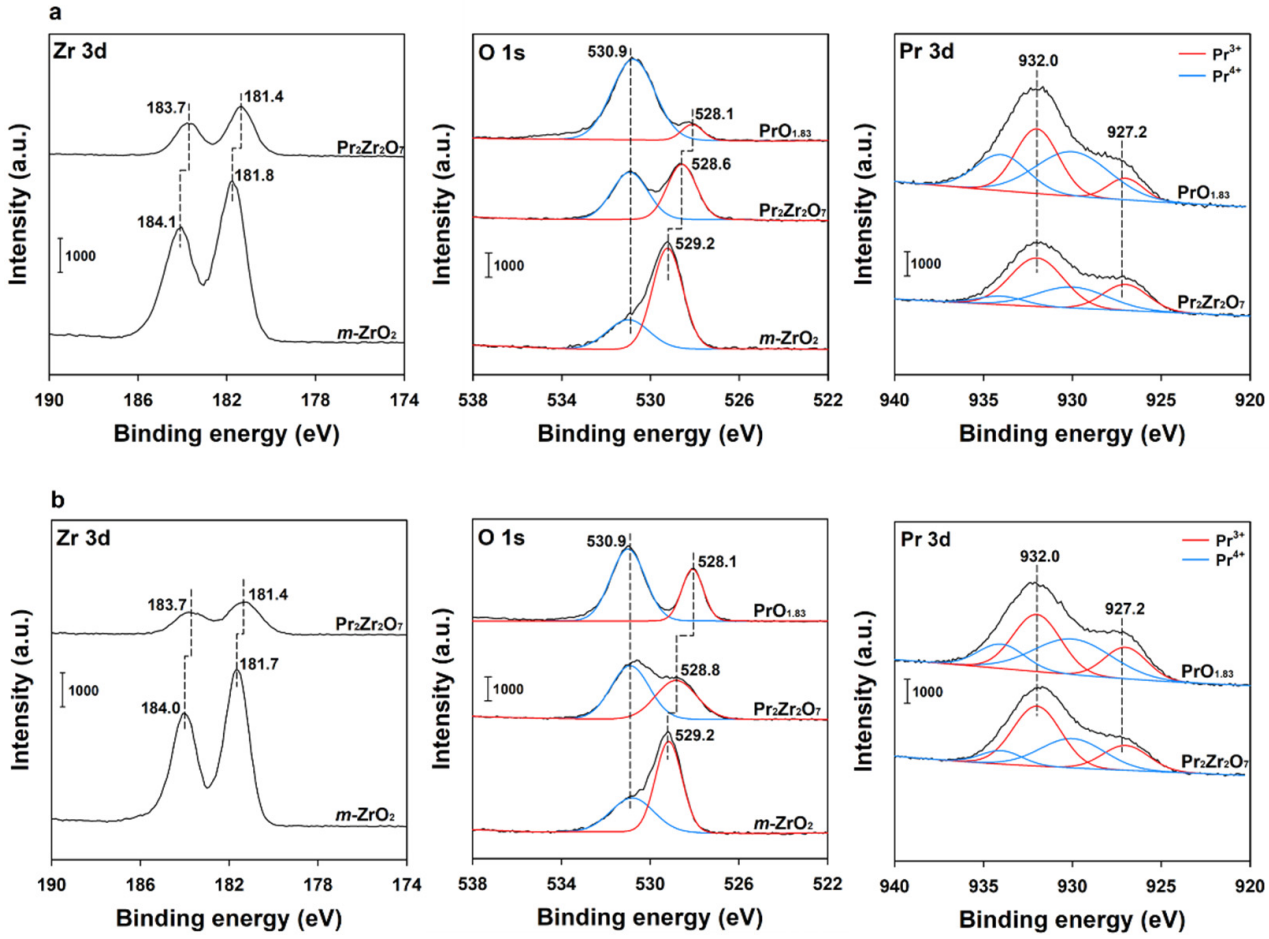

Figure 2. XPS spectra of (**a**) support materials and (**b**) supported Cu catalysts. Each panel represents the regions of Zr 3d (**left**), O 1s (**middle**), and Pr 3d (**right**).

To confirm the presence of oxygen vacancy, Raman spectra were acquired for the three support materials. In general, fluorite-type CeO_2 shows two absorption bands in the ranges of 400–500 and 500–600 cm^{-1} that can be assigned to a symmetric breathing mode of the oxygen ions coordinating the tetravalent cations and a defect mode caused by oxygen vacancy, respectively [24,35–37]. Similar absorption bands centered at 430 and 540 cm^{-1} were observed for $PrO_{1.83}$ and $Pr_2Zr_2O_7$, but not for *m*-ZrO_2 (Figure 3). The Raman intensity ratio I_{540}/I_{430} was lower for $Pr_2Zr_2O_7$ than for $PrO_{1.83}$. This indicates that $Pr_2Zr_2O_7$ has a lower concentration of oxygen vacancy than pure $PrO_{1.83}$ because of the stabilizing effect of Zr ions, which is in agreement with the finding identified in the XPS O 1s spectra.

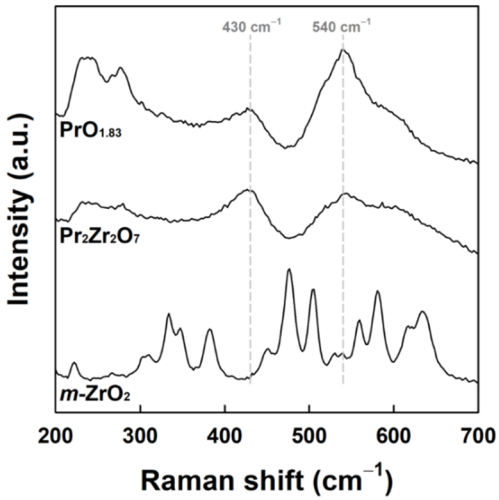

Figure 3. Raman spectra of m-ZrO_2, $Pr_2Zr_2O_7$, and $PrO_{1.83}$.

2.2. Activity and Stability Comparison of Supported Cu Catalysts

Activity tests were conducted under the reaction conditions reported in our previous works [11,12]. The products including isopropanol (IPA), 2-heptanone ($2C_7$-one), 6-undecanone ($6C_{11}$-one), 2-heptanol ($2C_7$-ol), and 6-undecanol ($6C_{11}$-ol) were quantified with respect to the molar selectivity of each species among all products converted from acetone. In particular, the mono-/di-coupling products ($2C_7$-one, $2C_7$-ol, $6C_{11}$-one, and $6C_{11}$-ol) were summed to represent the total yield of cross-coupling products. Thus, the conversion of acetone was mainly used for activity comparison. Note that the cross-coupling products are formed by the consumption of one and two moles of butanol per mole of acetone, which makes it complicated to understand the conversion of butanol (listed in Table S1).

Among the prepared catalysts, Cu/m-ZrO_2 showed the lowest acetone conversion of 73.9%, along with the butanol conversion of 56.2%. The yields of the cross-coupling products (C_7 and C_{11}) were only 27.9%, while the IPA selectivity was high at 59.6% (Figure 4). The activity results of Cu/m-ZrO_2 are explained by the lower basicity (i.e., lower oxygen vacancy) and higher Cu dispersion compared to the other catalysts (Table 1). Additionally, its acidity can affect the poor yield of coupling products. The highly dispersed copper particles of Cu/m-ZrO_2 (Cu dispersion of 30.4%) not only affect butanol dehydrogenation into butyraldehyde but also convert acetone into IPA by the hydrogen transferred by the dehydrogenation reaction. Moreover, the mono-coupling products, $2C_7$-one (selectivity = 19.9%) and $2C_7$-ol (selectivity = 14.8%), were more selectively formed than the di-coupling products (selectivities of $6C_{11}$-one and $6C_{11}$-ol = 3.0%), attributed to the lower basicity of Cu/m-ZrO_2 because CO_2 desorption was observed at ca. 100 °C (Figure 5a). This was also identified in m-ZrO_2 (Figure 5b).

Table 1. Characteristics of the prepared Cu catalysts.

Catalyst	Cu loading [a] (wt %)	S_{BET} [b] (m^2 g^{-1})	V_p [b] (cm^3 g^{-1})	S_{Cu} [c] (m^2 g^{-1})	D_{Cu} [c] (%)	N_{CO_2} [d] (μmol g^{-1})
Cu/*m*-ZrO_2	5.75	22.4	0.07	3.9	30.4	37 (33)
Cu/$PrO_{1.83}$	5.63	29.7	0.23	2.5	19.3	785 (418)
Cu/$Pr_2Zr_2O_7$	5.61	13.6	0.03	2.0	15.8	187 (109)

[a] Measured by inductively coupled plasma–mass spectrometry (ICP-MS) analysis. [b] Brunauer–Emmett–Teller (BET) surface area (S_{BET}) and pore volume (V_p) measured by N_2 physisorption. BET isotherms and pore size distribution curves are presented in Figure S1. [c] Cu surface area (S_{Cu}) and dispersion (D_{Cu}) measured by N_2O reactive frontal chromatography experiments. [d] Number of adsorbed CO_2 measured by CO_2 temperature-programmed desorption experiments, where the value in parentheses indicates the N_{CO_2} of Cu-free support materials.

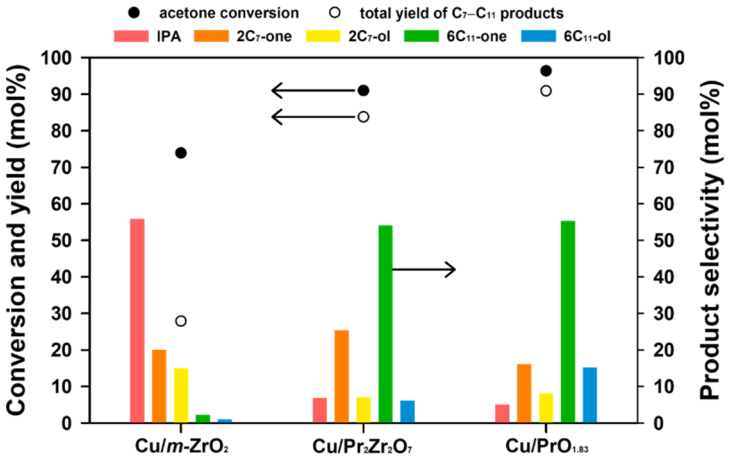

Figure 4. Catalytic performance of Cu/m-ZrO_2, Cu/$Pr_2Zr_2O_7$, and Cu/$PrO_{1.83}$ in the cross-coupling of acetone with butanol. Reaction conditions: 20 g reactant with the butanol/acetone mole ratio of 2, catalyst 1 g, 240 °C, and 20 h.

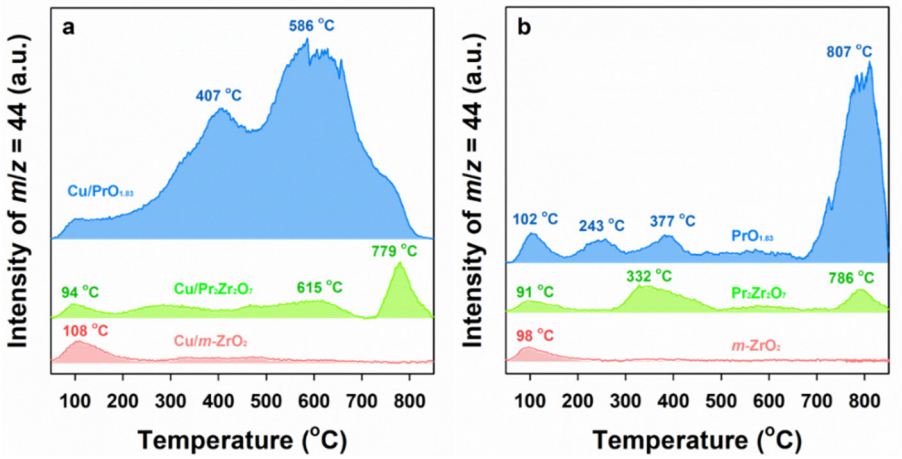

Figure 5. CO_2 temperature-programmed desorption (TPD) profiles of (**a**) supported Cu catalysts and (**b**) support materials.

In contrast, the conversion of acetone over Cu/$PrO_{1.83}$ was high at 96.4% while the selectivity to IPA was only 4.9%. The conversion of butanol was 91.0% and the cross-coupling reaction preferentially took place, which was examined by the higher selectivity of $6C_{11}$-one (55.2%) and $6C_{11}$-ol (15.1%). As a result, the yield of C_7 and C_{11} was 3-fold larger for Cu/$PrO_{1.83}$ (90.9%) than for Cu/*m*-ZrO_2, possibly caused by the high basicity of Cu/$PrO_{1.83}$ resulting from the large amount of oxygen vacancy, in which acid sites were nearly absent. As presented in Figure 5, $PrO_{1.83}$ and Cu/$PrO_{1.83}$ showed broad CO_2 desorption profiles, where the peaks below 200 °C, between 200 and 500 °C, and above 500 °C are assigned to weak base OH groups, medium-strength metal–oxygen pairs, and low-coordination oxygen anions, respectively [22]. On the other hand, Cu/$Pr_2Zr_2O_7$ exhibited acetone conversion of 91.0%, lower than Cu/$PrO_{1.83}$. The selectivity of the di-coupling products (59.9%) was also slightly lower due to the lower basicity (i.e., lower oxygen vacancy) of Cu/$Pr_2Zr_2O_7$ than Cu/$PrO_{1.83}$. However, the formation of IPA was suppressed in comparison with Cu/*m*-ZrO_2 because of the lower Cu dispersion of Cu/$Pr_2Zr_2O_7$ (15.8%). Therefore, the mixed oxide $Pr_2Zr_2O_7$ prefers the coupling of acetone with butanol to the Cu-catalyzed hydrogenation of acetone to IPA. Furthermore, it should be highlighted that Cu/$Pr_2Zr_2O_7$ shows superior catalytic performance to the previously reported Cu/CeO_2–ZrO_2 [11] and Cu–CeO_2 [12].

Catalyst stability in this reaction is an important issue, as studied with Cu/CeO_2–ZrO_2 and Cu–CeO_2. After the activity tests under the reaction conditions stated in Figure 4, the spent catalysts were characterized by XRD analysis. The phase change was remarkable for $Cu/PrO_{1.83}$ in which $PrO_{1.83}$ was transformed into $PrOHCO_3$ (JCDPS #24-1006), as shown in Figure 1b. This was confirmed when the calcined $PrO_{1.83}$ support was subjected to the identical reaction conditions (not shown here for brevity). A similar transformation was reported for Cu–CeO_2, showing the formation of $CeOHCO_3$ from CeO_2 [12]. This carbonate species is attributed to metal complexation with CO_2 that is possibly produced by ketonization of the dehydrogenation product of butanol (i.e., butyraldehyde). Therefore, $PrO_{1.83}$ is not considered to be useful due to its inferior stability, although the cross-coupling activity was high.

On the other hand, the XRD patterns of the fresh and spent Cu/m-ZrO_2 were similar, except the intensity of Cu (111) reflection at the 2θ of 43.3° was slightly weakened, meaning that copper leaching occurs during the reaction. The leaching was confirmed by the ICP result (ca. 140 ppm) obtained from the reaction mixture collected after the reaction over Cu/m-ZrO_2. Such catalyst instability was rarely observed with $Cu/Pr_2Zr_2O_7$ because the fresh and spent forms showed nearly identical XRD patterns. The same observation was found with the supported Cu on $Pr_2Zr_2O_7$ prepared with the Pr/Zr mole ratio of 3:7 though showing the C_7–C_{11} yield of 45.6%. This is a beneficial effect of mixing ZrO_2 with praseodymium oxide in terms of catalyst stability. Therefore, the $Cu/Pr_2Zr_2O_7$ with the Pr/Zr mole ratio of 5:5 is suggested to be an effective and stable catalyst in the coupling of acetone with butanol.

2.3. Catalytic Performance of $Cu/Pr_2Zr_2O_7$ with Different Cu Loadings

The acetone conversion and product selectivities were investigated in terms of Cu loading (Figure 6). In the case of Cu-free $Pr_2Zr_2O_7$ tested in the coupling of butyraldehyde with acetone at the mole ratio of 2 and 240 °C for 20 h, the acetone conversion approached 72.4%, but a variety of unidentified products were obtained along with IPA. This means that the cross-coupling reaction does not involve free aldehyde but rather the acyl species adsorbed on surface Cu particles, which was previously confirmed with Cu/CeO_2–ZrO_2 [11]. As the Cu loading increased from 1 to 5 wt %, the conversion of acetone became higher, from 82.6% to 91.0%, along with the increase in butanol conversion from 60.2% to 82.6%. More importantly, the cross-coupling products were more formed (i.e., increase in C_7–C_{11} yield from 66.9% to 83.8%), whereas the selectivity of IPA decreased from 17.7% to 6.7%. This means that the rates of butanol dehydrogenation and subsequent reaction with acetone are improved at a higher Cu loading, leading to fast consumption of the surface acyl species towards coupling products. This clearly explains the crossover in the selectivities of $2C_7$-one (decrease from 36.6% to 25.3%) and $6C_{11}$-one (increase from 32.4% to 53.9%) with the increase in Cu loading.

On the other hand, the reduced IPA selectivity may result from the diminished transfer hydrogenation function of copper particles. Thus, temperature-programmed reduction (TPR) experiments were carried out for $Pr_2Zr_2O_7$ and $CuO/Pr_2Zr_2O_7$. As displayed in Figure 7, $Pr_2Zr_2O_7$ shows a broad reduction in 300 to 550 °C that is attributed to the reduction of Pr^{4+} to Pr^{3+} [15]. For $CuO/Pr_2Zr_2O_7$ with 1 wt % Cu, this reduction peak was also found with an additional peak in 160–290 °C, indicating H_2 reduction of dispersed copper oxide particles. A similar reduction profile was obtained in 3 wt % $Cu/Pr_2Zr_2O_7$: the low-temperature peak was more intense because of the high Cu content, while the high-temperature peak moved toward a low temperature. These two events were merged in the range 200–420 °C for the sample with 5 wt % Cu loading, because H_2 reduction is generally retarded for large CuO particles. This explains the lowered transfer hydrogenation activity of 5 wt % $Cu/Pr_2Zr_2O_7$. The increase in Cu particle size with the Cu content was confirmed by Cu reflections in XRD patterns (Figure S2) and transmission electron microscopy (TEM) results (Figure S3). When calculated from the diffraction peak of Cu (111) using the Scherrer equation, Cu particle size increased from 37 (1 wt % Cu) to 42 nm (5 wt % Cu).

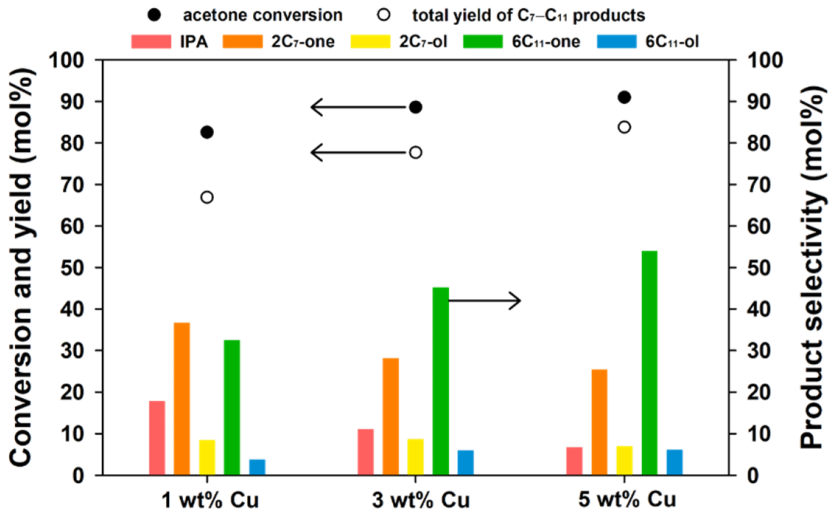

Figure 6. Catalytic performance of $Cu/Pr_2Zr_2O_7$ (1, 3, and 5 wt % Cu) in the cross-coupling of acetone with butanol. Reaction conditions: 20 g reactant with the butanol/acetone mole ratio of 2, catalyst 1 g, 240 °C, and 20 h.

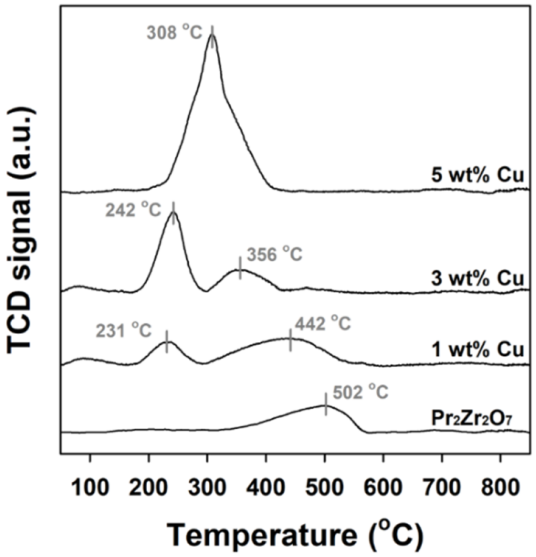

Figure 7. TPR profiles of the calcined $Pr_2Zr_2O_7$ and $CuO/Pr_2Zr_2O_7$ of 1, 3, and 5 wt % Cu.

2.4. Catalytic Performance of $Cu/Pr_2Zr_2O_7$ with Respect to the Reaction Time and H_2O Content

The activity and product distribution of 5 wt % $Cu/Pr_2Zr_2O_7$ were studied as the reaction time varied (Figure 8). In the early time of 3 h, the conversion of acetone was 66.9%, while IPA and $2C_7$-one were the major products with selectivities of 28.9% and 43.4%, respectively. As the experiment progressed to 12 h, the acetone conversion increased to 90.6%, and $6C_{11}$-one (48.6%) and $6C_{11}$-ol (6.0%) were more formed with the decreases in the selectivities of IPA (9.8%) and $2C_7$-one (26.0%). This product distribution was slightly changed for the longer reaction period—specifically, the total yield of C_7–C_{11} was 83.8% and 85.9% at 20 and 24 h, respectively. Therefore, the reaction needs to be performed for at least 20 h to preferentially produce the C_{11} products instead of the IPA and C_7 products.

Additionally, the effect of water on the activity of 5 wt % $Cu/Pr_2Zr_2O_7$ was investigated because water is released by the cross-coupling reaction and is detrimental to catalytic activity [11]. Figure 9 shows that the activity and product distribution strongly depend on the content of water added into the reaction. When the water content was 3 and 5 wt % relative to the reactant mixture (i.e., acetone plus butanol), the acetone conversion and C_7–C_{11} yield were maintained at the levels of 91% and 82 ± 2%, respectively.

However, the selectivity of $6C_{11}$-one declined from 53.9% (no water) to 42.6% (5 wt % H_2O), whereas the selectivities of the C_7 products ($2C_7$-one and $2C_7$-ol) increased from 32.2% (no water) to 38.9% (5 wt % H_2O) and that of IPA also increased to 10.9%. In other words, water lowers the cross-coupling ability of $Cu/Pr_2Zr_2O_7$ and shifts the catalytic function towards the transfer hydrogenation of acetone to IPA. This can be explained by the probable reason that water blocks the oxygen vacancy of $Pr_2Zr_2O_7$, thereby reducing its basic strength [31,34], and forms surface oxidized copper species (i.e., Cu^{1+}) resulting in the formation of a Cu^0/Cu^{1+} interface favorable for enhanced hydrogenation activity [12]. This phenomenon was more obvious when more than 5 wt % H_2O was added; the major product was not $6C_{11}$-one but $2C_7$-one under these conditions. Moreover, the acetone conversion and C_7–C_{11} yield were greatly reduced to ca. 80% and 63 ± 1%, respectively, at the water content of 10 wt %. Particularly, the decrease in the C_7–C_{11} yield was attributed to the higher selectivity of IPA (21%). Therefore, $Cu/Pr_2Zr_2O_7$ is resistant to water of up to 5 wt % relative to the reactant mixture. When compared with the catalysts reported in the literature, this catalyst has an advantage over Ni–MgO–SiO_2 [9] and is comparable to Ni–MgO–SBA-16 [38].

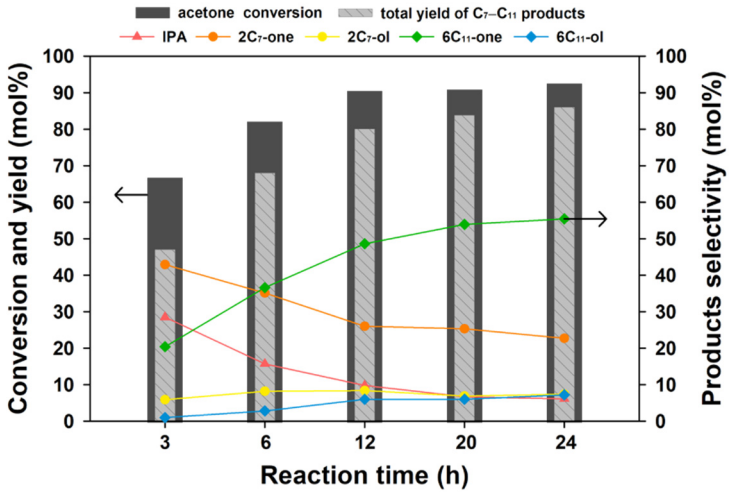

Figure 8. Effect of reaction time on the catalytic performance of 5 wt % $Cu/Pr_2Zr_2O_7$ in the cross-coupling of acetone with butanol. Reaction conditions: 20 g reactant with the butanol/acetone mole ratio of 2, catalyst 1 g, and 240 °C.

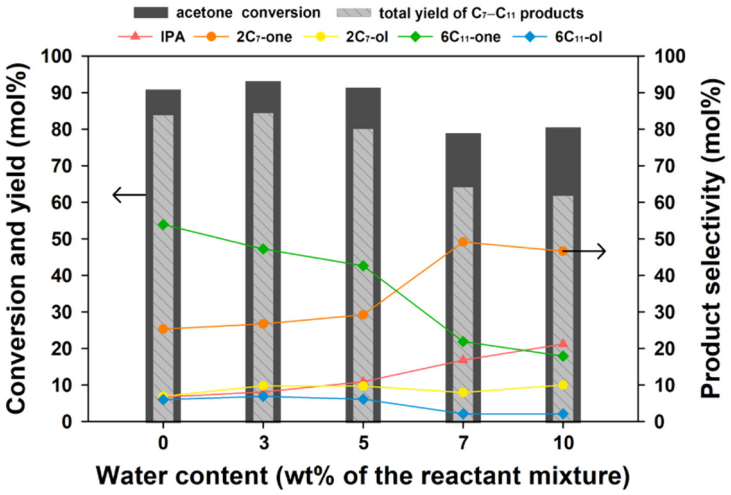

Figure 9. Effect of water on the catalytic performance of 5 wt % $Cu/Pr_2Zr_2O_7$ in the cross-coupling of acetone with butanol. Reaction conditions: 20 g reactant with the butanol/acetone mole ratio of 2, catalyst 1 g, 240 °C, and 20 h.

2.5. Catalyst Recyclability of $Cu/Pr_2Zr_2O_7$

The spent $Cu/Pr_2Zr_2O_7$ catalyst was separated from the product mixture by filtration, dried at 105 °C, and activated by H_2 reduction at 250 °C. When this catalyst was tested under the same conditions as in the first cycle, the acetone conversion and product distribution were negligibly changed, resulting in the C_7–C_{11} yield of 84.0% (cycle 2 in Figure 10a). When the spent catalyst was subjected to the identical post-treatment, the acetone conversion dropped to 78.7%, along with the decrease in C_7–C_{11} yield to 64.2% (cycle 3 in Figure 10a). Moreover, the selectivity of $6C_{11}$-one was significantly declined, and vice versa for IPA and the C_7 products. This was also observed in further cycles only when H_2 activation was performed.

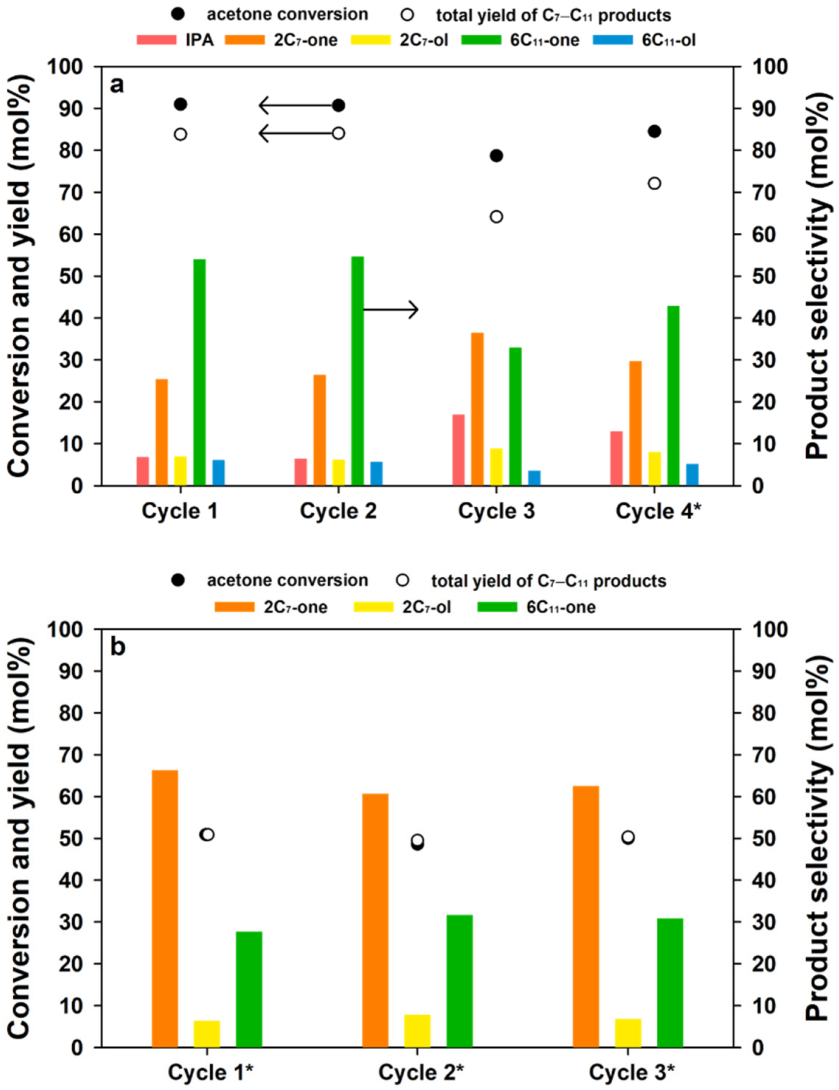

Figure 10. Catalytic performance of 5 wt % $Cu/Pr_2Zr_2O_7$ in the cross-coupling of acetone with butanol in recycle runs. Reaction conditions: 20 g reactant with the butanol/acetone mole ratio of 2, catalyst 1 g, (**a**) 240 °C and (**b**) 200 °C, and 20 h. * For cycle 4 in panel (**a**) and for all the cycles in panel (**b**), the catalyst was obtained by calcination at 400 °C and H_2 reduction at 250 °C, which is different from the other cycles using only H_2 reduction at 250 °C for 2 h.

Thus, the spent catalysts obtained after cycles 2 and 3 were characterized by XRD analysis. As depicted in Figure 11, the diffraction peaks of $PrOHCO_3$ were detected in the patterns of the as-obtained samples and even the samples reduced at 250 °C, which is attributed to the oxygen vacancy of $Pr_2Zr_2O_7$, even though the quantity is lower than

$PrO_{1.83}$. Once again, the presence of $PrOHCO_3$ is harmful to the reaction. To recover the catalytic activity, calcination at 400 °C, which is usually performed after impregnation of copper species on the prepared supports, was added before H_2 activation. As a result, the reflections of $PrOHCO_3$ disappeared by oxidation of hydroxycarbonate species (Figure 11). This catalyst showed improved acetone conversion and C_7–C_{11} yield of 84.5% and 72.1%, respectively (cycle 4 in Figure 10a). When the same two-step catalyst regeneration protocol was used for three consecutive runs at 200 °C, the acetone conversion and C_7–C_{11} yield were maintained at 50.0% (Figure 10b).

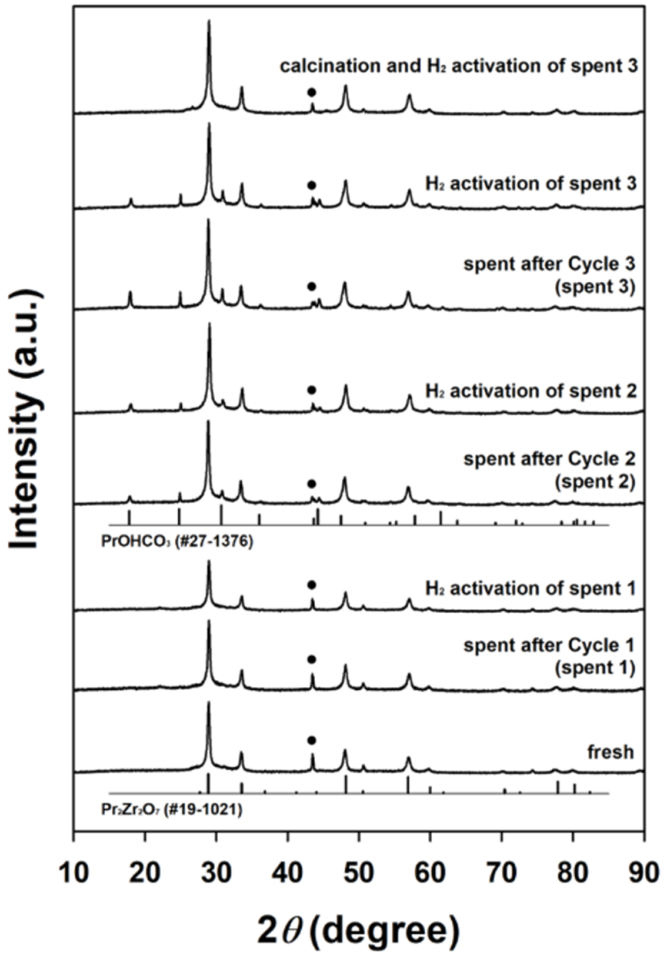

Figure 11. XRD of the fresh and spent catalyst of 5 wt % $Cu/Pr_2Zr_2O_7$ in recycle runs. The symbol represents the diffraction peak of Cu (111) and the bar plots are the representative reference XRD patterns of $PrOHCO_3$ and $Pr_2Zr_2O_7$.

2.6. Catalytic Performance of $Cu/Pr_2Zr_2O_7$ in the Cross-Coupling of the ABE Mixture

Finally, 5 wt % $Cu/Pr_2Zr_2O_7$ was tested in the conversion of an ABE mixture with the mole ratio of 2.3:3.7:1, which is the general product composition obtained by anaerobic fermentation of real biomass. The acetone conversion was measured to be about 94%. Aside from the products formed from the mixture of acetone and butanol, 2-pentanone ($2C_5$-one) and 4-nonanone (4-C_9-one) were produced by the mono-coupling of acetone with ethanol and the di-coupling of acetone with ethanol and butanol, respectively (Figure 12). The overall yield of C_5–C_{11} products was 82%, which is nearly equivalent to the yield of C_7–C_{11} products (82 ± 2%) obtained from the acetone–butanol mixture.

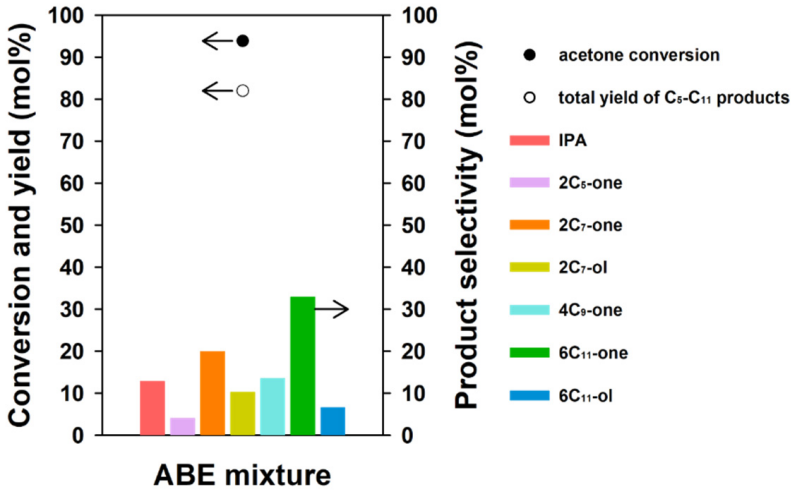

Figure 12. Catalytic performance of 5 wt % $Cu/Pr_2Zr_2O_7$ in the cross-coupling of the ABE mixture. Reaction conditions: 20 g reactant with the acetone/butanol/ethanol mole ratio of 2.3:3.7:1, catalyst 2 g, 240 °C, and 24 h.

3. Materials and Methods

3.1. Preparation of Supported Cu Catalysts

Three support materials were synthesized by precipitation. For the synthesis of praseodymia–zirconia, a solution of $Pr(NO_3)_3 \cdot 6H_2O$ (19.8 g; Sigma-Aldrich, Munich, Germany) and $ZrO(NO_3)_2 \cdot xH_2O$ (10.6 g; Strem Chem., Newburyport, MA, USA) in 150 mL of distilled water, with a metal concentration of 0.6 M, was added dropwise into 100 mL of an aqueous ammonia solution (25–28 wt %; Daejung Chem., Seoul, Korea) within 20 min. The resulting suspension was aged at room temperature, filtered three times, and dried at 105 °C overnight. After sieving to 200 µm, the dried co-precipitate was calcined at 600 °C for 5 h. The same procedure was used for the synthesis of zirconia and praseodymia. Then, an aqueous $Cu(NO_3)_2 \cdot 3H_2O$ solution was impregnated onto the synthesized support samples, where the nominal copper loading was set at 5 wt %. Finally, the supported copper catalysts were calcined at 400 °C for 5 h and finally activated by H_2 reduction at 250 °C for 2 h prior to the activity test. The H_2 reduction temperature was determined from the preliminary results that the activity of $Cu/Pr_2Zr_2O_7$ was negligibly changed when the catalyst was reduced at 250, 350, and 400 °C.

3.2. Catalyst Characterization

XRD analysis was performed with a Rigaku MINI Flex 600 (Rigaku Corp., Spring, TX, USA) using a Cu Kα radiation source at 40 kV and 15 mA with the step size of 0.02°. The BET surface area and pore volume were measured by N_2 physisorption using a Micromeritics 3Flex (Micromeritics Instrument Corp., Norcross, GA, USA) after degassing at 200 °C for 2 h. ICP-MS analysis was performed in an iCAP RQ spectrometer (Thermo Fisher Scientific, Waltham, MA, USA) to measure actual Cu content. XPS analysis was performed with a K-alpha plus spectrometer (Thermo Fisher Scientific, Waltham, MA, USA) with a monochromatic Al Kα source of 1486.6 eV. All of the spectra were obtained with a pass energy of 50 eV and a step size of 0.1 eV, followed by calibration based on the standard C 1s binding energy of 284.6 eV. The Raman spectrometer DXR-3xi (Thermo Fisher Scientific, Waltham, MA, USA) was used with 532 nm laser excitation generated by a diode-pumped solid state laser with a sample power of 1 mW. Raman spectra were obtained in the range 50–3400 cm^{-1} with a resolution of 2 cm^{-1}. Transmission electron microscopy (TEM) images were taken in a JEM-ARM200F microscope (JEOL USA, Inc., Peabody, MA, USA) operated at 200 kV after a sample in ethanol was dropped onto a 300-mesh copper grid and dried at 60 °C under vacuum overnight.

To measure Cu surface area and Cu dispersion, N_2O reactive frontal chromatography experiments were performed using a BELCAT-B coupled with a mass detector (BEL Japan, Inc., Toyonaka, Japan). After reduction of a sample (ca. 50 mg) at 250 °C for 2 h with 10% H_2/Ar (30 cm^3 min^{-1}) and cooling to 40 °C under He, 1% N_2O/He (5 cm^3 min^{-1}) was introduced and the released nitrogen (m/z = 28) was measured by a mass detector. The calculation was based on the reaction stoichiometry of Cu to oxygen (Cu/O = 2), and the copper surface density of 1.46 × 10^{19} Cu atoms m^{-2}. CO_2-TPD experiments were performed using a BELCAT-B instrument in line with a mass detector. For the calcined samples (50 mg), pretreatment was conducted at 250 °C for 2 h with a flow of 10% H_2/He (50 cm^3 min^{-1}) to yield metallic copper particles, and cooled to 35 °C under He. After 5% CO_2 in H_2 was supplied at 35 °C for 30 min and purged for 2 h with He, CO_2 desorption in He flow (30 cm^3 min^{-1}) was recorded while the sample was heated to 850 °C at a rate of 10 °C min^{-1}. For support samples, all the steps were identically performed, except the pretreatment at 250 °C for 2 h in He flow. TPR experiments were conducted in an Autochem 2910 instrument (Micromeritics Instrument Corp., Norcross, GA, USA). After pretreatment at 400 °C (for Cu catalysts) or 600 °C (for supports) for 3 h in 10% O_2/He, the temperature increased to 850 °C at a rate of 5 °C min^{-1} in a 10% H_2/Ar flow of 50 cm^3 min^{-1}.

3.3. Activity Tests for the Cross-Coupling of Acetone with Butanol

The reaction was performed in a stainless steel autoclave reactor (100 cm^3) charged with the prepared Cu catalyst of 1.0 g, acetone of 97 mmol, and butanol of 194 mmol. After N_2 purging five times, the reactor was heated to a certain temperature and maintained for a desired period under N_2, where the reactor pressure reached 25 bar. Similarly, the ABE mixture was used for the coupling reaction using acetone (51 mmol), butanol (81 mmol), and ethanol (22 mmol). After the reaction run was complete, the reactor was cooled to room temperature in order to condense the species that can exist as vapor phase under reaction conditions. The product mixture was separated from the catalyst via a syringe filter of 0.45 μm diameter and then mixed with cyclohexane and analyzed with a YL6100 gas chromatograph (Younglin Instrument, Anyang, Korea) equipped with an HP-INNOWAX column (50 m × 0.2 mm × 0.4 μm) and a flame ionization detector. The conversion of acetone was calculated by subtracting the initial mole of acetone by the mole of acetone remaining after the reaction.

4. Conclusions

We demonstrated the potential of fluorite-type praseodymia–zirconia (i.e., $Pr_2Zr_2O_7$) support in the Cu-catalyzed conversion of the acetone–butanol mixture and, furthermore, the acetone–butanol–ethanol mixture. A solid solution of the two metal oxide components was achieved by co-precipitation, which could lead to two effects: (1) stabilizing the structure of the less stable $PrO_{1.83}$ by the more stable *m*-ZrO_2 and (2) reducing the basicity of the more basic $PrO_{1.83}$. The latter was supported by the result that the selectivity of the di-coupling products was lower with Cu/$Pr_2Zr_2O_7$ than with Cu/$PrO_{1.83}$, and their activity difference was not significant. The former was consistent with the measured stability of Cu/$Pr_2Zr_2O_7$ showing little structural change under the tested conditions. Thus, Cu/$Pr_2Zr_2O_7$ was tolerant to water of up to 5 wt % relative to the substrate, and recyclable when calcination and H_2 reduction were accompanied. Consequently, the $Pr_2Zr_2O_7$ solid solution coupled with Cu metal can be used for efficient production of fuel precursors such as branched ketones and alcohols by the coupling of acetone with linear aliphatic saturated alcohols.

Supplementary Materials: The following is available online at: https://www.mdpi.com/article/10.3390/catal12101279/s1, Table S1: Conversion of butanol measured under different reaction conditions, where the reactant was 20 g with the butanol/acetone mole ratio of 2 and the catalyst used was 1 g. Figure S1: N_2 physisorption results of Cu/*m*-ZrO_2, Cu/$PrO_{1.83}$, and Cu/$Pr_2Zr_2O_7$ listed in Table 1: (a) BET isotherms and (b) pore size distribution curves. Figure S2: XRD patterns of the reduced Cu/$Pr_2Zr_2O_7$ of 1, 3, and 5 wt % Cu. The diffraction peak of Cu (111) is represented by

the square symbol. Figure S3: TEM images, Cu EDS mapping images, and line scanning results (obtained by tracking the orange line in the first image): (a) 1Cu/$Pr_2Zr_2O_7$, (b) 3Cu/$Pr_2Zr_2O_7$, and (c) 5Cu/$Pr_2Zr_2O_7$.

Author Contributions: Data curation, S.L., M.K. and J.-H.L.; conceptualization, S.L., M.K. and Y.-W.S.; methodology, S.L. and M.K.; validation, S.L. and M.K.; investigation, S.L., M.K., J.-H.L. and S.H.K. (S.L.: catalyst synthesis, characterization, and catalytic experiments, M.K.: catalyst characterization and catalytic experiments, J.-H.L.: catalyst characterization, S.H.K.: catalytic experiments); visualization, S.L., M.K. and J.-H.L.; supervision, Y.-W.S.; writing—original draft preparation, S.L., M.K., J.-H.L., J.H.B. and Y.-W.S.; writing—review and editing, S.L., M.K., J.-H.L., J.H.B. and Y.-W.S.; project administration, Y.-W.S.; funding acquisition, Y.-W.S. All authors have read and agreed to the published version of the manuscript.

Funding: This work was financially supported by the program titled "Technology Development Program to Solve Climate Changes" of the National Research Foundation of Korea under the Ministry of Science, ICT & Future Planning, Republic of Korea (NRF-2020M1A2A2080856), and by the Basic Science Research Program through the National Research Foundation of Korea under the Ministry of Education, Republic of Korea (NRF-2016R1A6A1A03013422).

Conflicts of Interest: The authors declare no conflict of interest.

References

1. Liberato, V.; Benevenuti, C.; Coelho, F.; Botelho, A.; Amaral, P.; Pereira, N., Jr.; Ferreira, T. *Clostridium* sp. as bio-catalyst for fuels and chemicals production in a biorefinery context. *Catalysts* **2019**, *9*, 962. [CrossRef]
2. Jones, D.T.; Woods, D.R. Acetone-butanol fermentation revisited. *Microbiol. Rev.* **1986**, *50*, 484–524. [CrossRef] [PubMed]
3. Maddox, I.S. The acetone–butanol–ethanol fermentation: Recent progress in technology. *Biotechnol. Genet. Eng. Rev.* **1989**, *7*, 189–220. [CrossRef] [PubMed]
4. Cho, C.; Jang, Y.S.; Moon, H.G.; Lee, J.; Lee, S.Y. Metabolic engineering of clostridia for the production of chemicals. *Biofuels Bioprod. Bioref.* **2015**, *9*, 211–225. [CrossRef]
5. Moon, H.G.; Jang, Y.-S.; Cho, C.; Lee, J.; Binkley, R.; Lee, S.Y. One hundred years of clostridial butanol fermentation. *FEMS Microbiol. Lett.* **2016**, *363*, fnw001. [CrossRef] [PubMed]
6. Anbarasan, P.; Baer, Z.C.; Sreekumar, S.; Gross, E.; Binder, J.B.; Blanch, H.W.; Clark, D.S.; Toste, F.D. Integration of chemical catalysis with extractive fermentation to produce fuels. *Nature* **2012**, *491*, 235–239. [CrossRef]
7. Sreekumar, S.; Baer, Z.C.; Gross, E.; Padmanaban, S.; Goulas, K.; Gunbas, G.; Alayoglu, S.; Blanch, H.W.; Clark, D.S.; Toste, F.D. Chemocatalytic upgrading of tailored fermentation products toward biodiesel. *ChemSusChem* **2014**, *7*, 2445–2448. [CrossRef]
8. Xu, G.; Li, Q.; Feng, J.; Liu, Q.; Zhang, Z.; Wang, X.; Zhang, X.; Mu, X. Direct α-alkylation of ketones with alcohols in water. *ChemSusChem* **2014**, *7*, 105–109. [CrossRef]
9. Zhu, Q.; Shen, C.; Wang, J.; Tan, T. Upgrade of solvent-free acetone–butanol–ethanol mixture to high-value biofuels over Ni-containing MgO–SiO_2 catalysts with greatly improved water-resistance. *ACS Sustain. Chem. Eng.* **2017**, *5*, 8181–8191. [CrossRef]
10. Fridrich, B.; Stuart, M.C.A.; Barta, K. Selective coupling of bioderived aliphatic alcohols with acetone using hydrotalcite derived Mg−Al porous metal oxide and Raney nickel. *ACS Sustain. Chem. Eng.* **2018**, *6*, 8468–8475. [CrossRef]
11. Kim, M.; Park, J.; Kannapu, H.P.R.; Suh, Y.-W. Cross-aldol condensation of acetone and *n*-butanol into aliphatic ketones over supported Cu catalysts on ceria-zirconia. *Catalysts* **2017**, *7*, 249. [CrossRef]
12. Kannapu, H.P.R.; Kim, M.; Jeong, C.; Suh, Y.-W. An efficient Cu–CeO_2 citrate catalyst for higher aliphatic ketone synthesis via alkali-free alkylation of acetone with butanol. *Mater. Chem. Phys.* **2019**, *229*, 402–411. [CrossRef]
13. Itoh, M.; Motoki, K.; Saito, M.; Iwamoto, J.; Machida, K. Lean NO_x reduction by hydrogen over Pt-supported rare earth oxide catalysts and their in situ DRIFTs study. *Bull. Chem. Soc. Jpn.* **2009**, *82*, 1197–1202. [CrossRef]
14. Maitra, A.M. Determination of solid state basicity of rate earth oxides by thermal analysis of their carbonates. *J. Therm. Anal.* **1990**, *36*, 657–675. [CrossRef]
15. Alcalde-Santiago, V.; Bailón-García, E.; Davó-Quiñonero, A.; Lozano-Castelló, D.; Bueno-López, A. Three-dimensionally ordered macroporous PrO_x: An improved alternative to ceria catalysts for soot combustion. *Appl. Catal. B Environ.* **2019**, *248*, 567–572. [CrossRef]
16. Sato, S.; Takahashi, R.; Sodesawa, T.; Igarashi, A.; Inoue, H. Catalytic reaction of 1,3-butanediol over rare earth oxides. *Appl. Catal. A Gen.* **2007**, *328*, 109–116. [CrossRef]
17. Borchert, Y.; Sonström, P.; Wilhelm, M.; Borchert, H.; Bäumer, M. Nanostructured praseodymium oxide: Preparation, structure, and catalytic properties. *J. Phys. Chem. C* **2008**, *112*, 3054–3063. [CrossRef]
18. Sato, K.; Imamura, K.; Kawano, Y.; Miyahara, S.; Yamamoto, T.; Matsumura, S.; Nagaoka, K. A low-crystalline ruthenium nano-layer supported on praseodymium oxide as an active catalyst for ammonia synthesis. *Chem. Sci.* **2017**, *8*, 674–679. [CrossRef]

19. Narula, C.K.; Haack, L.P.; Chun, W.; Jen, H.-W.; Graham, G.W. Single-phase PrO_y–ZrO_2 materials and their oxygen storage capacity: A comparison with single-phase CeO_2–ZrO_2, PrO_y–CeO_2, and PrO_y–CeO_2–ZrO_2 materials. *J. Phys. Chem. B* **1999**, *103*, 3634–3639. [CrossRef]
20. Stefanik, T.S.; Tuller, H.L. Nonstoichiometry and defect chemistry in praseodymium-cerium oxide. *J. Electroceram.* **2004**, *13*, 799–803. [CrossRef]
21. Borchert, H.; Frolova, Y.V.; Kaichev, V.V.; Prosvirin, I.P.; Alikina, G.M.; Lukashevich, A.I.; Zaikovskii, V.I.; Moroz, E.M.; Trukhan, S.N.; Ivanov, V.P.; et al. Electronic and chemical properties of nanostructured cerium dioxide doped with praseodymium. *J. Phys. Chem. B* **2005**, *109*, 5728–5738. [CrossRef] [PubMed]
22. Tankov, I.; Pawelec, B.; Arishtirova, K.; Damyanova, S. Structure and surface properties of praseodymium modified alumina. *Appl. Surf. Sci.* **2011**, *258*, 278–284. [CrossRef]
23. Li, H.; Li, K.; Zhu, X.; Du, Y.; Wei, Y.; Zhai, K.; Wang, H. Synthesis of mesoporous $Pr_xZr_{1-x}O_{2-\delta}$ solid solution with high thermal stability for catalytic soot oxidation. *J. Ind. Eng. Chem.* **2017**, *54*, 126–136. [CrossRef]
24. Martínez-Munuera, J.C.; Zoccoli, M.; Giménez-Mañogil, J.; García-García, A. Lattice oxygen activity in ceria-praseodymia mixed oxides for soot oxidation in catalysed gasoline particle filters. *Appl. Catal. B Environ.* **2019**, *248*, 567–572. [CrossRef]
25. Subramanian, M.A.; Aravamudan, G.; Subba Rao, G.V. Oxide pyrochlores—A review. *Prog. Solid State Chem.* **1983**, *15*, 55–143. [CrossRef]
26. Yamamura, H.; Nishino, H.; Kakinuma, K.; Nomura, K. Crystal phase and electrical conductivity in the pyrochlore-type composition systems, $Ln_2Ce_2O_7$ (*Ln* = La, Nd, Sm, Eu, Gd, Y and Yb). *J. Ceram. Soc. Jpn.* **2003**, *111*, 902–906. [CrossRef]
27. Yamamura, H.; Nishino, H.; Kakinuma, K. Ac conductivity for $Eu_2Zr_2O_7$ and $La_2Ce_2O_7$ with pyrochlore-type composition. *J. Ceram. Soc. Jpn.* **2004**, *112*, 553–558. [CrossRef]
28. Matović, B.; Maletaškić, J.; Yoshida, K.; Yano, T. Synthesis, characterization and sintering of fluorite and pyrochlore-type compounds: $Pr_2Zr_2O_7$, $Sm_2Zr_2O_7$ and $PrSmZr_2O_7$. *Mater. Today Proc.* **2019**, *16*, 156–162. [CrossRef]
29. Xu, X.; Liu, F.; Han, X.; Wu, Y.; Liu, W.; Zhang, R.; Zhang, N.; Wang, X. Elucidating the promotional effects of niobia on SnO_2 for CO oxidation: Developing an XRD extrapolation method to measure the lattice capacity of solid solutions. *Catal. Sci. Technol.* **2016**, *6*, 5280–5291. [CrossRef]
30. Paunović, N.; Dohčević-Mitrović, Z.; Scurtu, R.; Aškrabić, S.; Prekajski, M.; Matović, B.; Popović, Z.V. Suppression of inherent ferromagnetism in Pr-doped CeO_2 nanocrystals. *Nanoscale* **2012**, *4*, 5469–5476. [CrossRef]
31. Kim, J.-S.; Na, C.W.; Kwak, C.-H.; Li, H.-Y.; Yoon, J.W.; Kim, J.-H.; Jeong, S.-Y.; Lee, J.-H. Humidity-independent gas sensors using Pr-doped In_2O_3 macroporous spheres: Role of cyclic Pr^{3+}/Pr^{4+} redox reactions in suppression of water-poisoning effect. *ACS Appl. Mater. Interfaces* **2019**, *11*, 25322–25329. [CrossRef] [PubMed]
32. Zhang, X.; Fang, X.; Feng, X.; Li, X.; Liu, W.; Xu, X.; Zhang, N.; Gao, Z.; Wang, X.; Zhou, W. $Ni/Ln_2Zr_2O_7$ (Ln = La, Pr, Sm and Y) catalysts for methane steam reforming: The effects of A site replacement. *Catal. Sci. Technol.* **2017**, *7*, 2729–2743. [CrossRef]
33. Al Kutubi, H.; Rassaei, L.; Olthuis, W.; Nelson, G.W.; Foord, J.S.; Holdway, P.; Carta, M.; Malpass-Evans, R.; McKeown, N.B.; Tsang, S.C.; et al. Polymers of intrinsic microporosity as high temperature templates for the formation of nanofibrous oxides. *RSC Adv.* **2015**, *5*, 73323–73326. [CrossRef]
34. Oemar, U.; Ang, M.L.; Chin, Y.C.; Hidajat, K.; Kawi, S. Role of lattice oxygen in oxidative steam reforming of toluene as a tar model compound over $Ni/La_{0.8}Sr_{0.2}AlO_3$ catalyst. *Catal. Sci. Technol.* **2015**, *5*, 3585–3597. [CrossRef]
35. Ahn, K.; Yoo, D.S.; Hari Prasa, D.; Lee, H.-W.; Chung, Y.-C.; Lee, J.-H. Role of multivalent Pr in the formation and migration of oxygen vacancy in Pr-doped ceria: Experimental and first-principles investigations. *Chem. Mater.* **2012**, *24*, 4261–4267. [CrossRef]
36. Westermann, A.; Geantet, C.; Vernoux, P.; Loridant, S. Defects band enhanced by resonance Raman effect in praseodymium doped CeO_2. *J. Raman Spectrosc.* **2016**, *47*, 1276–1279. [CrossRef]
37. D'Angelo, A.M.; Chaffee, A.L. Correlations between oxygen uptake and vacancy concentration in Pr-doped CeO_2. *ACS Omega* **2017**, *2*, 2544–2551. [CrossRef]
38. Gong, Y.; Shen, C.; Wang, J.; Wu, C.; Tan, T. Improved selectivity of long-chain products from aqueous acetone–butanol–ethanol mixture over high water resistant catalyst based on hydrophobic SBA-16. *ACS Sustain. Chem. Eng.* **2019**, *7*, 10323–10331. [CrossRef]